E-20

ОБЪЕДИНЕННЫЙ
ИНСТИТУТ
ЯДЕРНЫХ
ИССЛЕДОВАНИЙ

Дубна

2710/2-72

E1 - 6534

I.V.Falomkin, M.M.Kulyukin, V.I.Lyashenko,
A.Mihul, F.Nichitiu, G.Piragino, G.Pontecorvo
Yu.A.Shcherbakov

PRELIMINARY PHASE SHIFT ANALYSIS FOR $\pi\,{}^4$He ELASTIC SCATTERING

ЛАБОРАТОРИЯ ЯДЕРНЫХ ПРОБЛЕМ

1972

E1 - 6534

I.V.Falomkin, M.M.Kulyukin, V.I.Lyashenko,
A.Mihul, F.Nichitiu, G.Piragino, G.Pontecorvo,
Yu.A.Shcherbakov

PRELIMINARY PHASE SHIFT ANALYSIS FOR $\pi\,^{4}He$ ELASTIC SCATTERING

ядерных исследований
БИБЛИОТЕКА

Introduction

At present there exist some experimental data on $\pi\ ^4He$ scattering in the region from 24 up to 153 MeV (table 1). The latest data on $\pi^{\pm}\ ^4He$ scattering have been obtained using the streamer chamber method at 100 MeV/1/.

Pion helium scattering at low energies is connected with two aspects: nuclear problems around the Λ_{33} resonance and extraction of the strong π -nucleus amplitude for determination of the pion form factor (at energies lower than 100 MeV). In the case of pion-nuclei scattering one of the most interesting aspects in this energy interval is a downward shift in the position of the first baryon resonance Λ_{33} . This shift is about 40 MeV for $\pi^-\ ^{12}C$ scattering,/2/ and a similar shift is expected for $\pi\ ^4He$ scattering/3/.

In this paper a preliminary phase shift analysis, performed as the first step for both the above aspects of pion helium scattering, is presented.

Formulation

The $\pi\ ^4He$ state is a pure $J=0$ and, therefore,we denote by $f(\theta,k)$ the total scattering amplitude parametrized in the usual way:

$$f^{\pm}(\theta,k)=\frac{1}{k}\Sigma(2\ell+1)\,e^{2i\tau_\ell^{\pm}}\,T_\ell\,P_\ell(\cos\theta)+f_c^{\pm}(\theta,k)\,. \qquad (1)$$

The pure nuclear amplitude is given by:

$$f_N(\theta,k)=\frac{1}{k}\Sigma(2\ell+1)\,T_\ell\;P_\ell\;(\cos\theta)\;, \qquad (2)$$

where k is the momentum in CMS, θ is the scattering angle in CMS, $P_\ell(\cos\theta)$ are ordinary Legendre polynomials, and $f_c^{\pm}(\theta,k)$ is the Coulmb amplitude. The partial wave amplitude T_ℓ may be expressed in terms of complex phase shifts $\Delta_\ell(k)$ (because in our energy interval there are inelastic channels) or in terms of real phase shifts $\delta_\ell(k)$ and inelasticity coefficients $\eta_\ell(k)$:

$$T_\ell(k)=Re\,T_\ell+i\,Jm\,T_\ell=\frac{\exp(2i\,\Delta_\ell)-1}{2i}=\frac{\eta_\ell\exp(2i\delta_\ell)-1}{2i} \qquad (3)$$

$$Re\,T_\ell=\frac{1}{2}\eta_\ell\sin(2\delta_\ell)$$

$$Im\,T_\ell=\frac{1}{2}(1-\eta_\ell\cos(2\delta_\ell))\,.$$

The Columb scattering amplitude is given by

$$f_c^{\pm}(\theta,k) = \frac{-n_c^{\pm}}{2k\sin^2\theta/2}\exp\left(-n_c^{\pm}\ln\sin^2\frac{\theta}{2} + 2i\,\tau_0^{\pm}\right), \qquad (4)$$

where the $\tau_\ell^{\pm}$ are the Coulomb phase shifts

$$\tau_\ell^{\pm} = \arg\Gamma\left(\ell + 1 + in_c^{\pm}\right),$$

and for small n_c the τ_ℓ are approximated by

$$\tau_0 = -0.5772 \quad n_c = -E n_c$$
$$\tau_1 = (1 - E)\, n_c$$
$$\tau_2 = \left(1 + \frac{1}{2} - E\right) n_c$$

E is the Euler constant, n_c is the Coulomb strength parameter:

$$n_c = \frac{Z_1 Z_2\, a\, m}{k} \quad \text{with} \quad m = \frac{m_1 m_2}{m_1 + m_2} \quad \text{and} \quad a = \frac{1}{137.036}$$

(in our energy interval $n = 0.024 \div 0.082 \ll 1$).
The differential cross section is expressed by

$$\frac{d\sigma}{d\Omega} = \left| f^{\pm}(\theta,k)\right|^2 \qquad (5)$$

and the elastic and total "pure" nuclear cross sections may be written as

$$\sigma_{el} = \frac{4\pi}{k^2}\sum(2\ell + 1)\left|T_\ell\right|^2, \qquad (6)$$

$$\sigma_{tot} = \frac{4\pi}{k^2}\sum(2\ell + 1)\,\mathrm{Im}\,T_\ell = \frac{4\pi}{k}\,\mathrm{Im}\,f_N(0,k). \qquad (7)$$

As was pointed out by Schiff[4], in the low energy region for π -nucleus interaction the expression (1) for the scattering amplitude is not sufficient and another amplitude - a distortion amplitude f_D , which is a model-dependent one, is necessary. In other words the nuclear amplitudes $f_N(\theta, k)$ will be different for $\pi^- \, {}^4He$ and $\pi^+ \, {}^4He$ scattering. This distortion amplitude is important for the S wave and hence for a good determination of the pion form factor. In our preliminary analysis we did not take into account a distortion amplitude, we considered $\pi^- \, {}^4He$ and $\pi^+ \, {}^4He$ scattering separately.

Experimental Data

The main bulk of experimental data on $\pi^\pm \, {}^4He$ scattering consists of elastic differential cross sections together with a few total cross section values (table 1). For the kinetic energy from 24 to 100 MeV 9 experiments have been performed by 4 groups of authors for $\pi^\pm$ elastic scattering on ${}^4He$ with a rough estimation of the total cross sections at 50, 58 and 65 MeV (Block's et al. data). At 110 and 153 MeV there are differential cross sections only for π^- on ${}^4He$ and also the total cross section data for 153 MeV. At 60 and 105 MeV two other measurements have been carried out for $\pi^- \, {}^4He$ scattering. The obtained differential cross sections are based on poor statistics and only estimations of the total and elastic cross sections are given.

Because of lack of knowledge of the total cross sections in our preliminary analysis we used only interpolated values of the elasticity ratio in a fit procedure. This ratio is a slowly decreasing function of energy:

$$x = \frac{\sigma_{el}}{\sigma_{tot}} \simeq 0.36$$ for 100 to 330 MeV (see fig.1).

Results

Prior to the phase shift analysis we made a fit of the differential cross sections data in terms of cosine and Legendre polynomial expansions. The information on the optimum number of partial waves required to fit the data was obtained using the F statistical test and the difference between the χ^2 of successively increased power of cosine. Table II shows an example of 97 MeV scattering data. The 95% point of the $F_{1,7}$ distribution is 5.59. Hence, the coefficients of the 6th and 5th for π^- and the 6th, 5th and 4th power polynomials for π^+ are not significant. All the cross sections data were refitted in polynomial Legendre expansions with 0.1,... up to 8 terms for a test of small contributions of the F wave (and D wave for 24 MeV):

$$\left(\frac{d\sigma}{d\Omega}\right)^* = \left(\frac{d\sigma}{d\Omega}\right)_{exp} - \left(\frac{d\sigma}{d\Omega}\right)_{coul.} = \frac{1}{k^2}\sum_{n=0}^{I_m} A_n(\cos\theta) \quad . \qquad (8)$$

$$I_m = 0,1,\dots, 8 \quad .$$

In Figure 2 the χ^2/N_{DF} of this fit for 51 MeV (π^+ and π^-), as well as for 153 MeV (π^-) are shown. A considerable decrease of the χ^2/N_{DF} was obtained from the fit with the Coulomb interference term $2\,Re(f_N^* f_c)$ (eq. 1). The χ^2/N_{DF} for the Legendre polynomial fit with 5 terms and the χ^2/N_{DF} obtained from a fit with eq. (1) are shown in table *III* . From all these fits it is possible to conclude that the dominant partial waves are the *S* and *P* for energies lower than 50 MeV, and the *S*, *P* and *D* waves up to 150 MeV. The small contribution of the *F* waves for medium energy (relative to the energy interval considered here) is probably caused by a large additional distortion amplitude. After many minimizations and a fit in a "chain way" (the output of one energy represents the inpit for the next energy) the most probable solution was found. Since both the colliding particles have a zero spin the Minami ambiguity will not appear and the single traditional ambiguity is in the sign, obtained by simultaneously reversing the signs of the real phase shifts. However, because of the strong influence of the Coulomb amplitude and the possibility of comparing the $\pi^-\,{}^4He$ and the $\pi^+\,{}^4He$ phase shift results, in this low energy region it is easy to remove the sign ambiguity. In addition, the simple impulse model theory for $\pi\,{}^4He$ scattering/12/ shows that in the low energy region (where predictions of this model are in agreement with the experimental data) the *S* wave is repulsive and the *P* wave is strongly attractive. In our analysis we assumed that the repulsive S solution is correct at low energy.

Because of a rough knowledge of the total cross section for $\pi^- \, {}^4He$ and $\pi^+ \, {}^4He$ a fit with the elasticity ratio $x = \sigma_{el} / \sigma_{tot}$ as an input for energies higher than 51 MeV was performed. The values of x were taken from linear interpolation between the experimental points.

A "chain method" was used for a smooth continuation of the phase shift results with energy. The mathematical procedure for minimization is a usual one, i.e. the least square method with a linearization method was used /15/ (program FUMILI). The false minima were removed by many minimizations with different inputs for each energy and by comparing the obtained total cross sections with experimental data.

For 153 MeV the simultaneous fit of the $d\sigma / d\Omega$ and the x ratio gives larger values of statistical errors for the parameters (solution 1), however, the free fit only for the $d\sigma / d\Omega$ with solution 1 as an input gives reasonable errors for the parameters and the total cross section values with the deviation from measured values being no more than 3 experimental errors.

In case of solution 1 there is evidence of a strong correlation between parameters and this explains large errors. That is why we give both the solutions and hope that a use of the regularization iterative Gauss-Newton process, which is now in progress /16/ will make it possible to obtain true errors for the fit with the x ratio.

In figures 3 and 4 the calculated elastic and total cross sections together with all other available experimental values are shown. The elastic cross sections are shown for two cases: extracted from phase shift analysis (eq. 6) - elastic nuclear cross section, and obtained by integration of eq. 8 - the cross section with Coulomb contribution.

Discussion

Figures 5,6 and 7 show the results for the real part of the phase shifts δ_ℓ and the inelasticity parameters η_ℓ (S,P and D wave). The S wave has a repulsive behaviour with an approximately linear dependence of δ_0 upon energy. The inelastic channels are open in the S wave for the whole energy interval and a dip in η_0 is observed between 110 and 153 MeV. The Argand diagram (Fig. 8a) for the S wave shows a part of the resonance circle (in the anti-clockwise direction) displaced to the left. This is a typical behaviour for an inelastic resonance in the presence of the repulsive non-resonant back-ground scattering /13/. In this case the real part of the phase shift does not go through any particular value, and η_0 has a minimum (observed for 110-153 MeV) but this may no longer coincide with the position of the resonance. The Argand diagram gives no evidence of the "size resonance" effect for ^4He in δ_0 predicted at $T_c \simeq 120\,MeV\ /\ A^{1/3} = 75\,MeV$ /17/. It may be connected with large absorption and/or the fact that the nucleus is too light in this case.

For the determination of the resonance and the background scattering parameters in the S wave, more accurate experimental data for this energy interval are required. The P wave (Fig. 6) shows a typical behaviour for an inelastic resonance with $\Gamma_{e\ell} < \frac{1}{2}\Gamma_{tot}$ in the presence of a small background. The phase shift δ_1 passes through zero at the resonance, and the inelasticity parameter η_1 has a small value in this region. The resonance circle in the Agrand diagrams passes below the centre of the unitary circle (Fig. 8b).

The D wave (Fig. 7) has the same behaviour as the P wave but with smaller values of δ_2. Therefore, it is interesting to note that the resonant aspects in $\pi\,^4He$ scattering appear at 140 MeV, i.e. at lower kinetic energy than in πN scattering. These aspects are present in all waves. In Figure 9 the extrapolated real amplitude at a zero angle $Re\, f_N(\theta^0)$ vs kinetic energy together with the dispersion predictions for $\pi\,^4He$ scattering /14/ (curves a and b), and the new dispersion predictions for $\pi\,^{12}C$ scattering /9/ (curve c) are presented. The curve d in this figure is an eye guiding line between the last two points. It is interesting to note that the line d is more or less paraliel to the new dispersion prediction for $\pi\,^{12}C$ scattering, and the similarity of the two curves may be a question of a scaling factor. The similarity between the dependences of the total cross sections upon the energy for the π^- -nucleus (with the number of nucleons $A \geq 4$) and the π -nucleon scattering is well known. The shape of these dependences may be empirically described by a scaling factor $A^{0.83}$ /14/. Figure 10 presents the plot of the ratio

$$a = \frac{Re\, f_N(\theta^0)}{Im\, f_N(\theta^0)}$$

vs kinetic energy. In the region of 50 MeV there is some evidence for a slight bump which may be connected with the inelastic thresholds. In Figures 9, 11, and 12 it is possible to observe some systematical discrepancies between Block's data (50, 58 and 60 MeV) and Crowe's data (51, 60, 68 and 75 MeV). Therefore, for the future analysis it is necessary to take into account the systematical errors for each experiment. These inconsistencies of the experiments in the region of the 60 MeV do not affect the general behaviour of the phase shifts or the bump at 50 MeV. It is necessary to perform new experiments not only at 150 MeV but also in the energy region of 50 to 80 MeV.

Conclusions

A preliminary phase shift analysis for $\pi\,{}^4He$ elastic scattering has been carried out in the energy region from 24 to 153 MeV. More experimental data are needed to eliminate some inconsistencies between the data obtained by different authors in the energy region 50 - 80 MeV. How -

ever, already now we can say that the energy behaviour of δ_ℓ and η_ℓ shows resonant aspects in the region of 140 MeV. All these aspects are reflection of the Δ_{33} resonance from πN scattering for the presence of a strong repulsive background scattering. The phases δ_1 and δ_2 pass through 0^0 which is typical for elasticity ratios $x < 0.5$ (in our case). The shift of the Δ_{33} position for ^4He is of the same order as in $\pi\ ^{12}C$ scattering. It is noteworthy that the presence of the resonance in ^4He is seen in all the waves, and in this case it would be interesting to find the exact resonant position for each wave. However, precise values of such positions may be determined on the basis of more data on $\frac{d\sigma}{d\Omega}$ and σ_{tot} obtained in the region from 100 to 200 MeV. Dispersion relation predictions for the real part of the forward amplitude do not agree with experimental data. The amplitude goes through zero at a lower energy.

The authors are grateful to V.P. Dzhelepov for supporting this work, L.I. Lapidus, P.S. Isaev and O.V. Dumbrais for interesting discussions.

References

1. I.V.Falomkin, M.M.Kulyukin, V.I.Lyashenko, F.Nichitiu, G.Piragino, G.B.Pontecorvo, Yu.A.Shcherbakov. Preprint Dubna P1-6131 (1971). Lettere al Nuovo Cimento. Vol.3, ser. 2, no. 11, p.461 (1972).
2. F.Binon, P.Duteil, J.P.Garron, J.Gorres, L.Hugon, J.P.Peigneux, C.Schmit, M.Spighel and J.P.Stroot. Nucl. Phys., B17, 168 (1970).

3. L.A.Charlton and J.M.Eisenberg. Ann. Phys. (N.Y.), 63, 286 (1971). T.E.O. Ericson and Jorg Hufner. Ref. TH 1247 CERN. M.P.Locher, O.Steinmann and N.Straumann. Nucl. Phys., B27, 598 (1971).

4. L.I.Schiff. Progr. Theor. Phys. (Kyoto) 400 (1965) Suppl..

5. M.E.Nordberg Jr. and K.F.Kinsey. Phys. Letters, 20, 962 (1966).

6. M.M.Block, I.Kenyon, J.Keren, D.Koetke, P.Malhotra, R.Walker and H.Winzeler. Phys. Rev., 196, 1074 (1968).

7. K.M.Crowe, A.Fainberg, J.Mtller and A.S.L. Parsons. Phys. Rev., 180,1349 (1969).

8. E.C.Fowler, W.B.Fowler, R.P.Shutt, A.M.Thornidike and W.L.Whittemore. Phys. Rev., 91, 135 (1953).

9. F.Binon, Z.Dimcovski, P.Duteil, M.Gouanere, L.Hugon, J.Jansen, J.P.Lagnaux, H.Palevsky, J.P.Peigneux, M.Spighel and J.P.Stroot. Contribution to 4th Int. Conf. on High Energy Physics and Nucl. Structure - Dubna 7-11 Sept. (1971) (preliminary results).

10. Yu.A.Budagov, P.F.Yermolov, E.A.Kushnirenko and V.I.Moskalev. JETP, 42, 1192 (1962).

11. M.S.Kozodaev, M.M.Kulyukin, R.M.Sulyaev, A.I.Filippov and Yu.A.Shcherbakov. JETP, 38, 409 (1960).

12. M.M.Block and D.Koetke. Nucl. Phys., B5,451 (1968). M.M.Block, I.Kenyon, J.Keren, D.Koetke, P.Malhotra, P.Mazur, R.Walker and H.Winzeler. Phys. Letters, 26B, 464 (1968).

13. A.Donnachie. Modern Developments in Hadron Physics in CERN 71-1.

14. T.E.O.Ericson and M.P.Lochev. CERN 69-30.

15. S.N.Sokolov and I.N.Silin. Preprint Dubna D810 (1961).

16. L.Alexandrov. Preprint Dubna P5.5515 (1970).

17. M.Ericson and M.Krell Phys. Letters, 38B,359 (1972).

Received by Publishing Department

on June 20, 1972.

Table I.

T MeV	Experimental Method	Differential cross section π^-	Differential cross section π^+	N of exp points	Total cross section	Ref number
24	Counter	x	x	8		5
50	bubble chamber	x	x	9	x	6
51	counter	x	x	15		7
58	bubble chamber	x	x	9	x	6
60	counter	x	x	15		7
60	diffusion chamber				x	8
65	bubble chamber	x	x	9	x	6
68	counter	x	x	15		7
75	counter	x	x	15		7
97	streamer chamber	x	x	14		1
105	diffusion chamber				x	8
110	spectrometer	x				9
153	diffusion chamber	x		23	x	10
273	diffusion chamber			15	x	11
330	diffusion chamber				x	11

Table II.

97 MeV	n=0	n=1	n=2	n=3	n=4	n=5	n=6	$F^{0.05}_{1,N_{OF}}$	χ^2	N_{OF}	Q
F	252.29	13.38	40.50	76.14	5.99	3.88	0.04	5.59	14.17	7	π^-
$\chi^2_n - \chi^2_{n-1}$	507.00	26.9	81.40	153.00	12.00	7.8	0.07			7	π^-
F	90.58	5.84	9.36	20.34	1.20	0.06	0.15	5.59	10.40	7	π^+
$\chi^2_n - \chi^2_{n-1}$	133.00	8.57	13.70	29.80	1.75	0.08	0.22			7	π^+

Table III.

T MeV	24	50	51	58	60	65	68	75	97	110	153	
π^- χ^2/N_{OF}	1.07	1.09	2.60	0.28	4.27	1.20	1.71	4.02	2.43	2.38	0.54	Leg. Pol. expansion $J=0,1,..4$
	0.75	1.26	1.89	0.12	3.60	0.92	1.35	3.10	2.32	2.30	0.53	Phase Shift Analysis
π^+ χ^2/N_{OF}	1.72	1.22	3.17	0.63	14.33	2.06	4.40	3.06	1.17	–	–	Leg. Pol. expansion $J=0,1,..4$
	0.91	1.16	2.24	0.5	6.70	2.02	2.80	2.70	1.10	–	–	Phase Shift Analysis

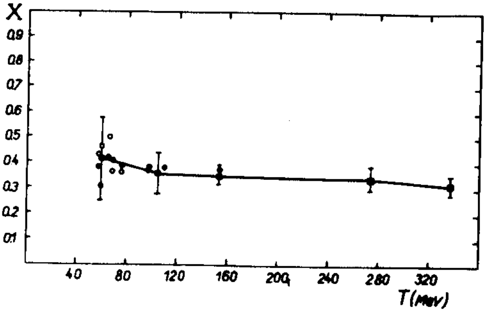

Fig. 1. Elasticity ratio x vs kinetic energy* ($x = \sigma_{el} / \sigma_{tot}$). ● π^- o π^+ from Phase Shift Analysis; ‡ experimental points.

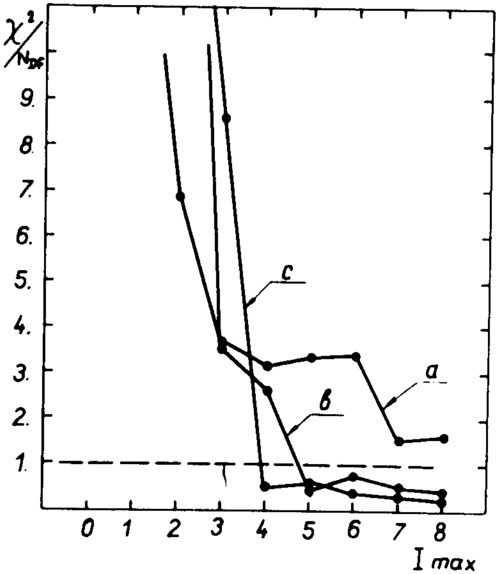

Fig. 2. χ^2 / N_{DF} vs I_{max} in multiple Legendre polynomial expansions for: a) 51 MeV (π^+); b) 51 MeV (π^-); c) 153 MeV (π^-).

*The curve is the eye guiding line.

Fig. 3. Elastic cross section *vs* kinetic energy.
▲ π^-, △ π^+ from Phase Shift Analysis; ● π^-, ○ π^+ from Legendre Polynomial expansion (*S* , *P* and *D* wave); experimental points.

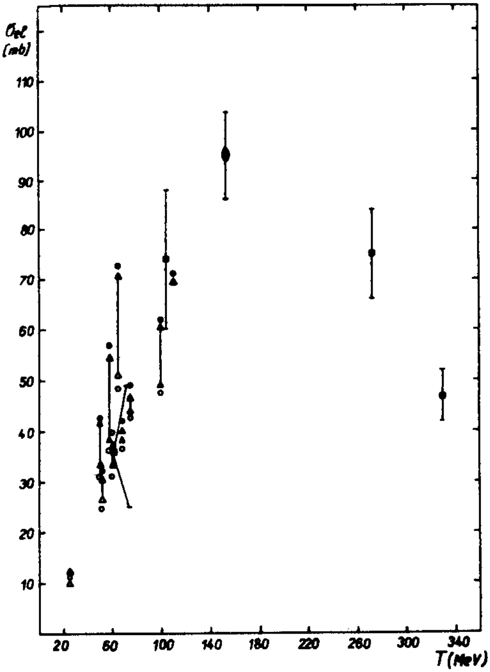

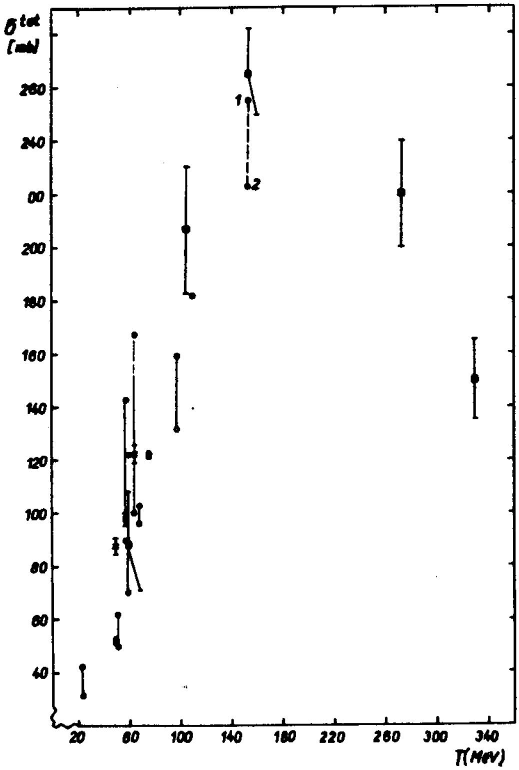

Fig. 4. Total cross section *vs* kinetic energy.
● π^-, ○ π^+ from Phase Shift Analysis; experimental points; experimental "nuclear"(Block's data) points.

Fig. 5. Real phase shift and inelasticity parameter vs kinetic energy* for the S wave (δ_0 and η_0).

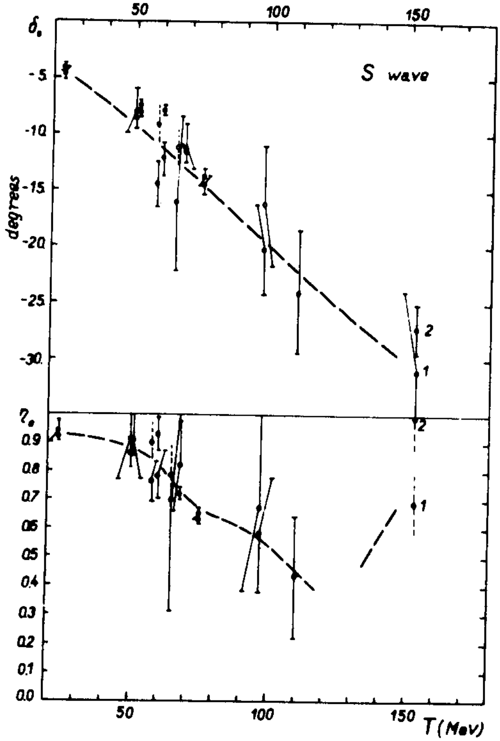

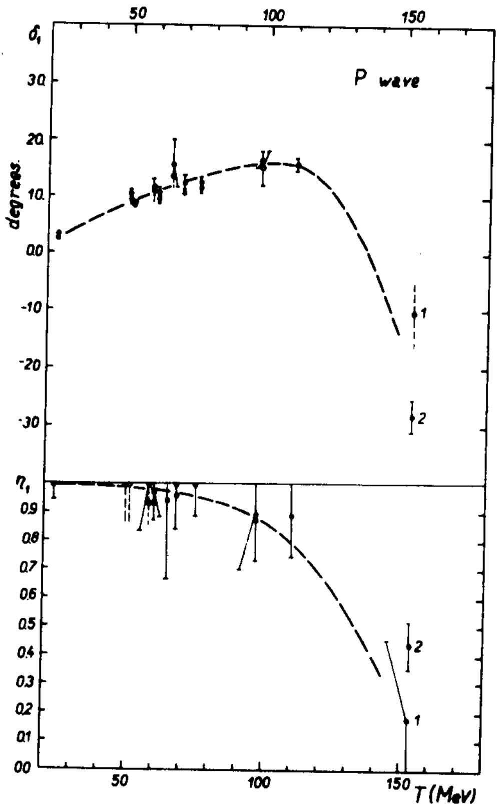

Fig. 6. P -wave (δ_1 and η_1).

*The curve is the eye guiding line.

Fig. 7. *D* -wave (δ_2 and η_2).

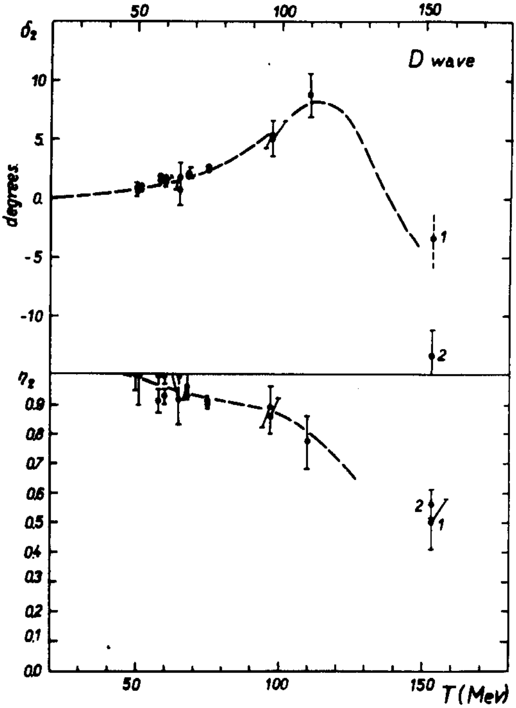

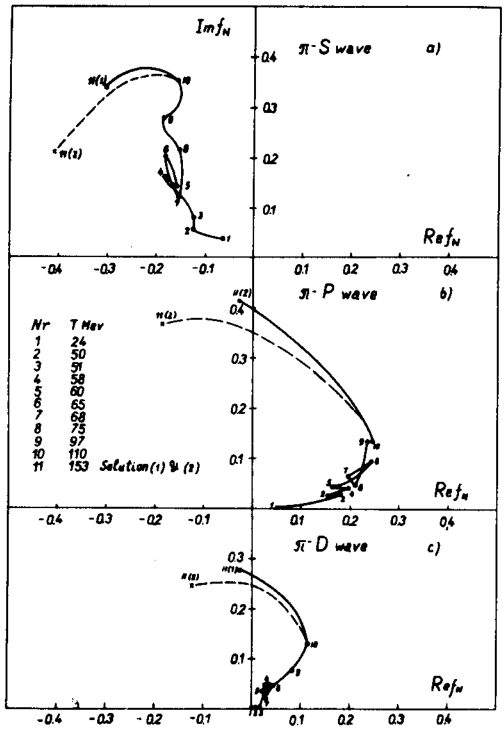

Fig. 8. Argand diagram for π^- ^4He *. a) *S* wave; b) *P* wave; c) *D* wave .

---

* The curve is the eye guiding line.

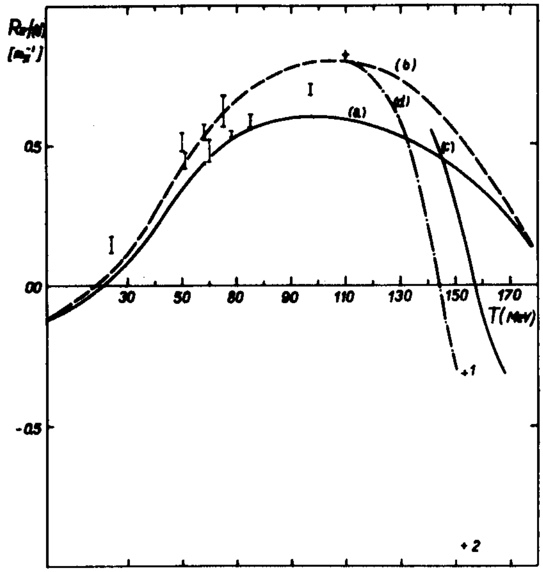

Fig. 9. $Re\ f_N(0^0)$ vs kinetic energy. The curve (a) is the dispersion prediction with the following input:/14/ I). $Im\ f(\omega) = (0.084 + 0.064\ k^2/m_\pi^2)\ m_\pi^{-1}$ for $0 < \omega < m_\pi + 10 MeV$. II), A smooth polynomial fit through the imaginary parts for ω < 1300 MeV. III) $\sigma(\omega) = (0.071 + 2.95\ MeV/\omega)^{1/2}$ for higher energies. IV) Subtraction constant $Re\ f(m_\pi) = (-0.132 \pm 0.003)\ m_\pi^{-1}$ The curve (b) shows the dispersion prediction for a $\sigma(\omega)$ increased by 3 standard deviations in the resonant region. The curve (c) shows the new dispersion prediction for $\pi^-\ ^{12}C$ elastic scattering/9/. The curve (d) is the guiding line between the last two points (without errors). For energies lower than 110 MeV, the error bars show the difference between π^- and π^+ results.

Fig. 10. The α ratio *vs* kinetic energy*. $\alpha = \frac{Re\, f_N(0^0)}{Im\, f_N(0^0)}$

I difference between π^- and π^+ results; + only for π^- .

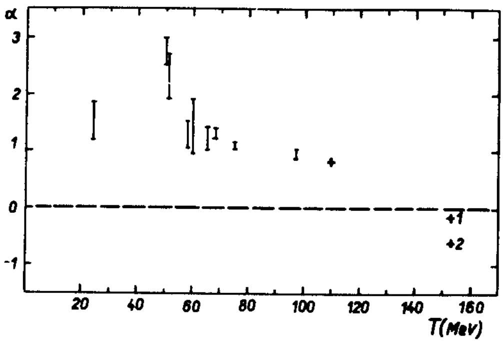

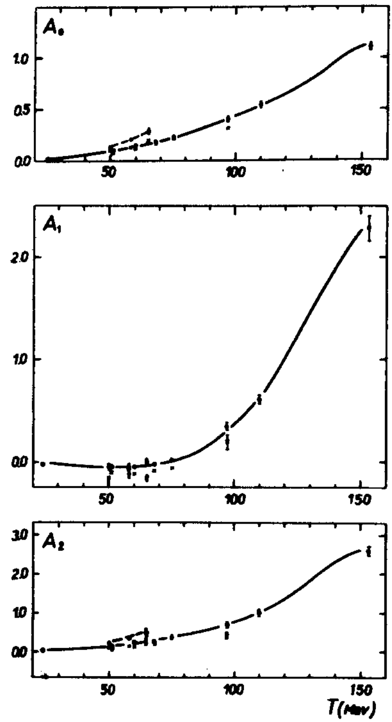

Fig. 11. Legendre polymial coefficients from fit with P_0 , ..., P_4 *. ⧳ - π^- , ⧳ - π^+

* The curve is the eye guiding line.

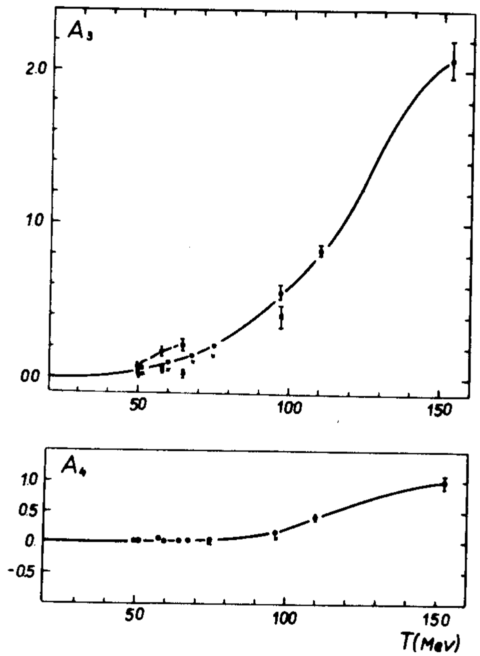

Fig. 12. Legendre polynomial coefficients from fit with P_0 , ... P_4 + .* ● – π^- , ✕ – π^+

---

* The curve is the eye guiding line.